J Fluoresc (2014) 24:137–141
DOI 10.1007/s10895-013-1279-6

ORIGINAL PAPER

Enhanced Fluorescence of Graphene Oxide by Well-Controlled Au@SiO_2 Core-Shell Nanoparticles

Cuiyan Li · Yihua Zhu · Siwen Wang · Xiaoqing Zhang · Xiaoling Yang · Chunzhong Li

Received: 3 April 2013 / Accepted: 18 July 2013 / Published online: 31 July 2013

Abstract Graphene and graphene derivatives, including graphene oxide (GO) and reduced GO (rGO), have attracted remarkable attention in different fields due to their unique electronic, thermal, and mechanical properties, whereas the fluorescence property is rarely been studied. This paper reports on metal-enhanced fluorescence Au@SiO_2 composite nanoparticles adsorbed graphene oxide nanosheets, where the silica-shell is used to control the distance between gold-core and fluorophore GO, and a positively charged polyelectrolyte poly(allylamine hydrochloride) (PAH) is used to adsorb the negatively charged silica-shell and GO by layer-by-layer assembly (LbL) approach. The silica-shell around the 80 nm gold-core can be well-controlled by ending the reaction at different times. Various analytical techniques were applied to characterize the morphology and optical characters of the as-prepared particles. A more than three-fold increase of the fluorescence intensity of GO was obtained.

Keywords Graphene oxide · Au@SiO_2 · Core-shell nanoparticles · Enhanced fluorescence

Introduction

Fluorescent carbon-based nanomaterals, such as nanotubes, fullerenes, and some nanoparticles, may be a more suitable alternative for in vivo biolabeling, bioimaging, and disease detection because of their superiority in chemical inertness, biocompatibility and low toxicity [1, 2]. During the recent several years, the discovery and extensive applications of graphene and graphene derivatives [3, 4], including graphene oxide (GO) and reduced GO (rGO), have attracted prodigious attention in different fields due to their unique electronic, thermal, and mechanical properties [5, 6]. Particularly, GO has received great interest because of its unique properties such as good dispersity in water and a substantial bandgap distinct from graphene and rGO [7]. Besides, as a low-cost precursor for bulk production of graphene [8], the retained two-dimensional structure and chemical functionality make GO attractive as nanocomposites applying in drug delivery, cell imaging, chemo/biosensing, biomediccal applications, and fluorescence quenching [9–13].

However, the fluorescent intensity of GO is relatively low in most reports [14, 15], but metal (such as gold or silver) has an enhanced effect on the fluorophore, as known as metal-enhanced fluorescence (MEF). It has been well established that the interactions between fluorophores and metal nanoparticles result in an increased photostability, fluorescence enhancement, and a decreased lifetime due to the increased rates of system radioactive decay [16, 17]. The fluorescence enhancement noted in these studies can stem from a mechanism of surface plasmon resonance [18, 19]. The spontaneous emission of light by molecules and atoms at nanostructured metallic surfaces is remarkably modified due to a complex interplay of enhancing and quenching physicochemical processes. On one hand, fluorescence enhancement can be promoted by surface plasmons excited in metal and by a modified density of photon states in a nanostructured surface; on the other hand, quenching processes include chemical bonding and non-radiative energy transfer from the luminescent species to the metal [20]. Excellent overlap of the GO absorption/emission spectrum with the scattering spectrum of the gold surface is required for effective surface plasmon resonance, while GO shows a broad absorption and emission spectrum, which provides a good overlap with the gold scattering spectrum. Importantly, the degree of metal-fluorophore interactions strongly depends on the distance between the fluorophore and the metal surface. There are various methods

C. Li (✉) · Y. Zhu · S. Wang · X. Zhang · X. Yang · C. Li
Key Laboratory for Ultrafine Materials of Ministry of Education,
School of Materials Science and Engineering,
East China University of Science and Technology,
130 Meilong Road, Shanghai 200237, China
e-mail: abuangle@126.com

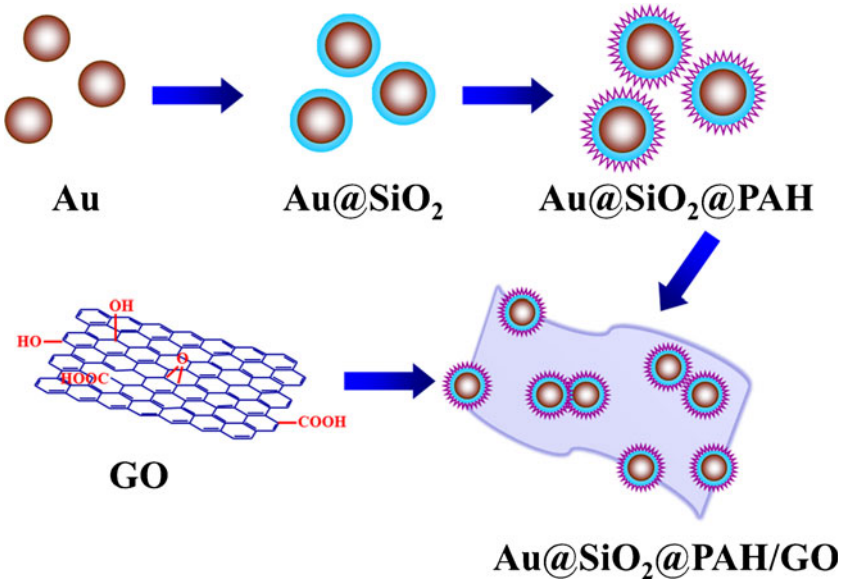

Fig. 1 Schematic representation of the preparation of $Au@SiO_2$ attached composite GO nanosheets

established to control this distance. Here we chose a simply controllable silica shell around the gold core to achieve this goal with several advantages: firstly, silica shell protects the gold core from ions present in biological media; secondly, silica layer offers the chemical inertness and the versatility need for the conjugation of biomolecules or fluorophores; thirdly, silica layer allows the distance dependent MEF phenomenon. In addition, since the silica-shell and GO are both negatively charged on their surface, a positively charged polyelectrolyte PAH, poly(allylamine hydrochloride), is used to attach $Au@SiO_2$ nanoparticles to GO by layer-by-layer (LbL) electrostatic assembly technology.

Herein, our concentric multilayer architecture features a gold core and a silica spacer shell around with a controlled and uniform thickness to prevent fluorescence quenching of GO by the metal at very close range. As represented in Fig. 1, the preparation of the composite nanostructures was undertaken in three steps: first, deposit a controllable silica layer onto the Au colloids to obtain $Au@SiO_2$ core-shell nanoparticles with different shell thicknesses; second, modify the silica surface with positively charged PAH; third, hybrid assembly between positively charged $Au@SiO_2$ nanoparticles and negatively charged GO by electrostatic interaction.

Experiments

Synthesize GO Nanosheets

The light-brown homogeneous GO nanosheets were easily synthesized from graphite power by a modified Hummers method [21, 22]. Briefly, put 1 g graphite powder into 40 mL concentrated H_2SO_4, then 5 g $KMnO_4$ was added gradually under stirring while keeping the temperature below 20 °C by continuous cooling. Successively, the mixture was stirred at 35 °C for 4.5 h in water bath and diluted with 100 mL deioned water, then stirred for 2 h. Afterward, 7 mL 30 % H_2O_2 was added to remove residual $KMnO_4$, meanwhile the color of the mixture turned into bright yellow. The solution was filtered and washed with 100 mL deioned water to remove th acid and the obtained filter cake was left overnight. Then disperse the filter cake in 100 mL deioned water and ultrasound oscillating for 1 h. The suspension was centrifuged at 1,000 rpm for 5 min to remove all visible particles (3 times). The sediment was discarded and the resulting supernatant containing light-brown GO was collected. Finally, the product was further purified by dialysis for a week to remove the remaining metal species. By sonicating dispersion under ambient conditions for 20 min, the homogeneous aqueous solution of GO was obtained, stable for several months.

Synthesize $Au@SiO_2$ Nanoparticles

The gold colloids with a diameter of 80 nm were purchased from BBInternational Company in UK to obtain uniform composite nanoparticles with well distribution. To deposit a silica shell on the gold core, we used a modified version of the well known Stöber's method. Normally, 4 mL gold colloids were dispersed in 20 mL isopropanol with 0.5 mL ammonia, then 1 mL tetraethyl orthosilicate (TEOS) solution (10 mM in isopropanol) was added to this solution to obtain a silica shell, where the different shell thickness was controlled by reaction time. At the beginning, 1 mL solution was taken out to be measured UV–vis spectra every 5 min Then the solution was centrifuged to get rid of extra TEOS to avoid further growth of silica shell and it was saved in the deioned water. After 1 h reaction, 1 mL solution was taken out to be treated the same way every 10 min; after 2 h the interval was 20 min, and after

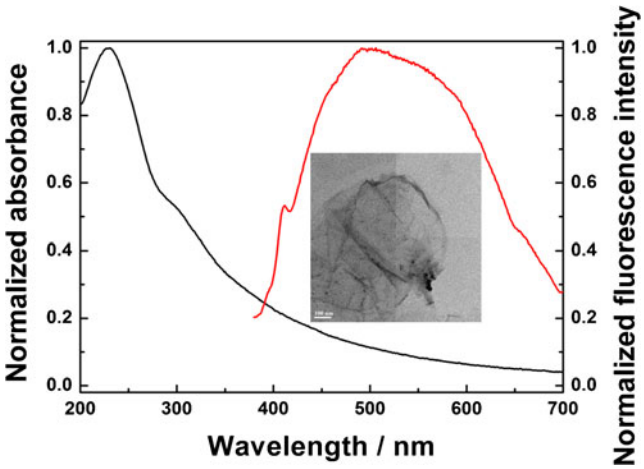

Fig. 2 The characteristics of the GO nanosheets: typical absorption spectra (*black line*), fluorescence emission spectra (*red line*), and the inserted TEM photograph (the scale bar is 100 nm)

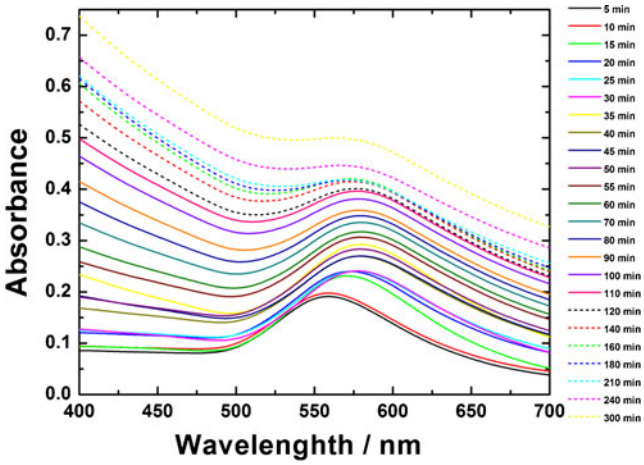

Fig. 3 UV–Vis absorption spectra of 80 nm gold particles (*black line*) and gold-silica core-shell nanoparticles with various shell thicknesses. The reaction time (T) is from 5 min to 5 h

3 h the interval was 30 min until 5 h, the end of the reaction. All the glass apparatus were immersed in *aqua regia* solution for 24 h before used.

Combine Au@SiO_2 Nanoparticles with GO Nanosheets

After centrifuging and washing with isopropanol, redisperse the Au@SiO_2 nanoparticles in 20 mL isopropanol, then add 0.5 mL PAH (1 %) to function the surface of positive charge. At last, the surface-modified particles were dispersed in GO solution at the volume ratio of 2:1 (3 mL Au@SiO_2 nanoparticles and 1.5 mL GO aqueous solution) and stirred at room temperature overnight. Then GO nanosheets were attached to the surface of the functionalized silica shells through electrostatic interaction, resulting in the targeted GO-attached Au@SiO_2 composite particles.

Results and Discussions

The integrative GO nanosheets with an average thickness of about 1 nm indicate a fully exfoliated GO single layer [23]. The oxygen-containing groups such as carboxyl, epoxide and hydroxyl groups linked GO nanosheets were characterized by UV–vis absorption spectra (the black line in Fig. 2). The GO displayed optical properties typical of chemically prepared GO, with two characteristic absorption peaks at 230 nm and 300 nm originating from π–π* transition of the C=C band and n–π* transition of the C=O band, respectively [14, 15, 24–26]. Despite a wide 2D size distribution of the GO from nanometers to micrometers, the GO dispersion in water showed good homogeneity and stability, as evidenced from the high negative Zeta potentials (−50.28 mV to −52.36 mV) [25]. A linear relationship between the absorption intensity and the concentration of GO in a wide range was verified. The GO gave fluorescence emission with a maximum at 506 nm upon excitation at 365 nm (the red line in Fig. 2), which was presumably assigned to the radiative recombination of electron–hole pairs localized within small sp^2 carbon domains embedded in the sp^3 matrix [26]. The homogeneously broadened fluorescence spectra of GO may reflect effects from various sizes of luminescent domains, and their multiple radiative recombination as well [27]. The general features of the fluorescence emission/excitation spectra of GO are distinct from those of luminescent carbon nanomaterials such as graphene quantum dots, carbon nanoparticles and single-walled carbon nanotubes (SWNTs) [28, 29]. The most likely luminescent species are emissive surface defects, as proposed tentatively by Sun et al. [30]. Negligible difference in spectral characteristics of the GO samples collected by different-speed centrifugation indicated a facile production of GO. The morphology of GO was examined with high-resolution transmission electron microscope (HR-TEM), which shows that the GO sheet was about 1×1 μm in size with occasional folds, crinkle s and rolled edges (Fig. 2 insert).

Figure 3 shows the UV–vis absorption shift trend spectra of citrate-protected gold colloids and of Au@SiO_2 particles with different silica shell thickness depending on the different reaction time from 5 min to 5 h. Initially, as the shell thickness increased, there is an increase in the intensity of the plasmon absorption band, as well as a red shift in the position of the absorption peak. Surface plasmon absorption bands were observed to red-shift from 553 nm (T=0 min) to 580 nm (T=45 min) when a silica shell (~20 nm) was deposited. This is due to the increase in the local refractive index around the particles. However, when the silica shell is larger, scattering becomes significant, giving rise to a strong increase in the absorbance at shorter wavelengths. This effect results a blue shift of the surface plasmon band and a weakening in the apparent intensity. After a stable fluctuation of peaks at 578 to 580 nm, as the shell thicknesses surpass 80 nm (T=120 min),

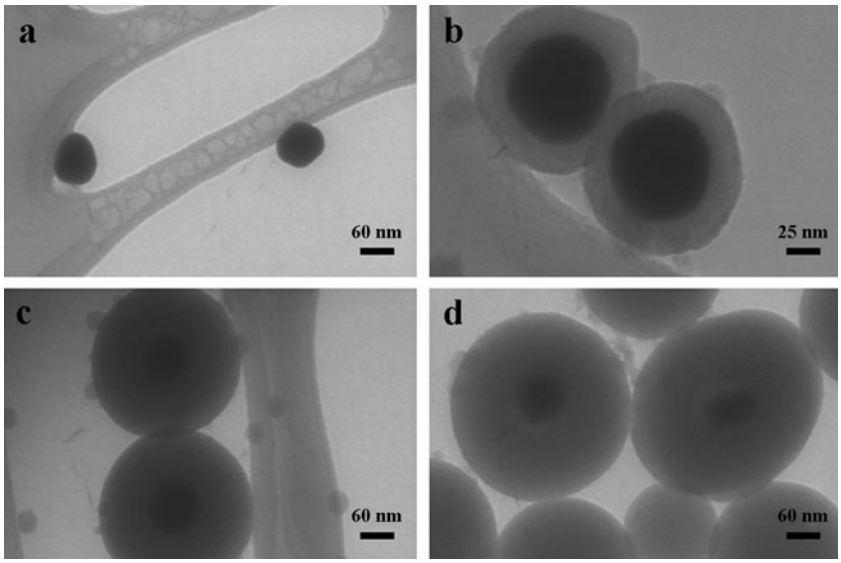

Fig. 4 **a** SEM photographs of Au colloids. **b**–**d** TEM images of $Au@SiO_2$ core-shell nanoparticles, where the silica shell thickness is 20, 80 and 120 nm, respectively

the scattering almost completely masks the surface plasmon band, the band blue-shifted back. Eventually, the final solution is very turbid and slightly pink in appearance with the silica thickness even reaches hundreds of nanometers (T=300 min). As we know, the surface plasmon absorption band in the visible area is very sensitive both to particle size and shape and to the properties of the surrounding medium [31], and its variation with various parameters has been extensively studied. In particular, the effect of silica shells with various thicknesses, and in various solvents, has been predicted by Mie theory which can verify the experimental data in this work.

Figure 4(a) indicates the citrate-protected gold nanoparticles have an average size of 80 nm. Uniform silica spacer shells were grown onto the gold nanoparticles as certified in Fig. 4(b–d) where typical $Au@SiO_2$ nanoparticles were presented. The thickness of the spacer shell was adjusted by the reaction time after TEOS was added in order to optimize the fluorescence enhancement. The thickness of the silica layers were 20±2 nm (T=45 min, Fig. 4b), 80±3 nm (T=120 min, Fig. 4c) and 120±5 nm (T=300 min, Fig. 4d), respectively. The nanoparticles with smooth surface and uniform silica shell thickness were also had a ordered array though there were occasional core-free silica spheres.

By measuring Zeta potential, the surface $Au@SiO_2$ nanoparticles was negatively charged (Zeta potential=−20.1 mV) at pH 7.8 because of the silane group on the silica shell. The surface of the PAH modified silica-coated gold nanoparticles was positively charged (Zeta potential=10.3 mV) at pH 7.8, which was because the alkylamines exist predominantly as positively charged $R\text{-}NH_3^+$ groups. Since the electrostatic interaction acts as the driving force for the assembly of GO onto amino modified nanoparticles, the targeted enhancemental luminescent $Au@SiO_2$ composite nanoparticles attached GO nanosheets with the negatively charged surface (Zeta potential=−18.6 mV) at pH 7.8 was successfully prepared. This charge was originated from the ionization of the carboxylic acid

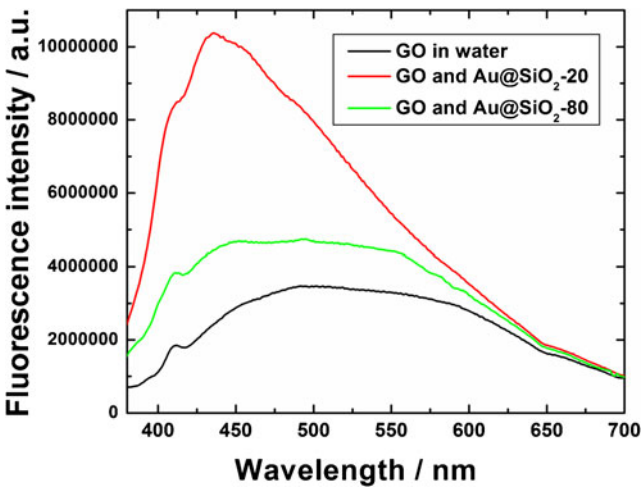

Fig. 5 Fluorescence emission intensity of GO nanosheets in water and in $Au@SiO_2$ nanoparticles with the silica-shell thickness of 20 nm and 80 nm, respectively (all volume ratio was 2:1)

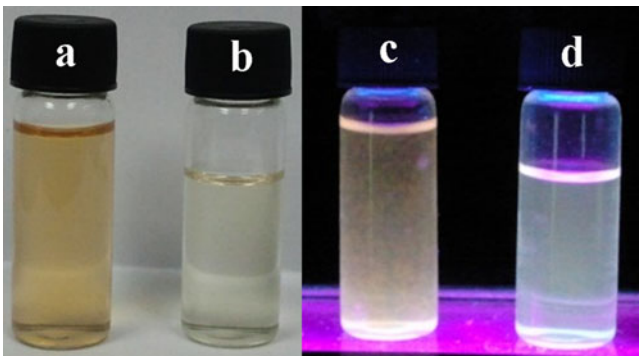

Fig. 6 Compare photos of GO in water (**a** and **c**) and GO attached with $Au@SiO_2$-20 (**b** and **d**) under nature light and (**a** and **b**) excited by 365 nm of ultravoilet light (**c** and **d**)

and hydroxy groups that were located on the surface of GO [32]. It can be deduced that GO were well-separated from each other on the silica surface, and the attachment was sufficiently strong that the GO remained attached to the silica shell when the nanoparticles were centrifuged out of the solution and redispersed.

Figure 5 shows the fluorescence emission intensity of GO in water and attached by Au@SiO_2 nanoparticles with different silica-shell thickness. Since Au@SiO_2-20 and Au@SiO_2-80 don't have fluorescent property, the fluorescence emission intensity of the three spectra all comes from the fluorescence of GO nanosheets. For the shell thickness of 20 nm (Au@SiO_2-20 for short), the fluorescence emission intensity of GO has a dramatically increase for more than three-folds, owing to the metal-enhancement. While for shell thickness of 80 nm (Au@SiO_2-80 for short), the fluorescence emission intensity of GO drops dramatically, because the silica-shell is too thick to make the gold-core affect fluorescent GO. Thus, in this work, 20 nm spacer thickness is an effective distance for metal-enhancement fluorescence. Though the intrinsic mechanism of GO luminescence is not yet fully understood, the metal-enhancement fluorescence was confirmed to be still applied when GO were used as fluorophores. Although many papers reported nanoballs by etching the metal-core as a comparison, we think them not scientific accurate when the nanoparticles were diluted by adding etchant and be washed away by incomplete centrifugation and redispersion. Therefore, we simply compared the fluorescent intensity of the composited nanoparticles attached GO nanosheets with GO diluted in the water with the same volume ratio.

We can see the MEF effect from Fig. 6 directly. When excited by 365 nm of ultravoilet light, from the upper parts of the two vials which are farther away from the excited light source, the GO nanosheets attached with Au@SiO_2-20 (Fig. 6d) were much brighter than GO diluted in the same volume of deioned water (Fig. 6c), with a obvious blue-shift from the light-brown colour of GO, which is accordance with the fluoresent spectra in Fig. 5.

Conclusions

In conclusion, we have investigated MEF effect of Au@SiO_2 nanoparticles attached GO nanosheets, where the silica-spacer thickness is adjusted to optimize the metal-fluorophores distance and the fluorescence enhancement. A more than three-fold increase of fluorescence intensity of GO was obtained. Further experiment with other types of metal or alloy nanostructures will allow clarifying the details of GO fluorescent property.

Acknowledgment We thank the National Natural Science Foundation of China (20925621, 20976054, and 21176083), the Special Projects for Nanotechnology of Shanghai (11nm0500800) the Fundamental Research Funds for the Central Universities (WD1013015 and WD1114005), and the Program for Changjiang Scholars and Innovative Research Team in University (IRT0825), and the Shanghai Leading Academic Discipline Project (project number: B502) for financial supports.

References

1. Sun YP, Zhou B, Lin Y, Wang W, Fernando KA, Pathak P, Meziani MJ, Harruff BA, Wang X, Wang H, Luo PG, Yang H, Kose ME, Chen B, Veca LM, Xie S-Y (2006) J Am Chem Soc 128:7756–7757
2. Hu SL, Niu KY, Sun J, Yang J, Zhao NQ, Du XW (2009) J Mater Chem 19:484–488
3. Geim AK, Novoselov KS (2007) Nat Mater 6:183–191
4. Campos-Delgado J, Romo-Herrera JM, Jia XT, Cullen DA, Muramatsu H, Kim YA, Hayashi T, Ren ZF, Smith DJ, Okuno Y, Ohba T, Kanoh H, Kaneko K, Endo M, Terrones H, Dresselhaus MS, Terrones M (2008) Nano Lett 8:2773–2778
5. Li XL, Wang XR, Zhang L, Lee SW, Dai HJ (2008) Science 319:1229–1232
6. Huang X, Zhou X, Wu S, Wei Y, Qi X, Zhang J, Boey F, Zhang H (2010) Small 6(4):513–516
7. Dreyer DR, Park S, Bielawski CW, Ruoff RS (2010) Chem Soc Rev 39:228–240
8. Li D, Muller MB, Gilje S, Kaner RB, Wallace GG (2008) Nat Nanotechnol 3:101–105
9. Liu Z, Robinson JT, Sun X, Dai H (2008) J Am Chem Soc 130:10876–10877
10. Scheuermann GM, Rumi L, Steurer P, Bannwarth W, Mulhaupt R (2009) J Am Chem Soc 131:8262–8270
11. Lu CH, Yang HH, Zhu CL, Chen X, Chen GN (2009) Angew Chem Int Ed 48:4785–4787
12. Liu Y, Liu C, Liu Y (2011) Appi Surf Sci 257:5513–5518
13. Yang X, Wang Y, Huang X, Ma Y, Huang Y, Yang R, Duan H, Chen Y (2011) J Mater Chem 21:3448–3454
14. Dong H, Gao W, Yan F, Ji H, Ju H (2010) Anal Chem 82:5511–5517
15. Chen J-L, Yan X-P (2011) Chem Commun 47:3135–3137
16. Aslan K, Huang J, Wilson GM, Geddes CD (2006) J Am Chem Soc 128:4206–4207
17. Aslan K, Holley P, Geddes CD (2006) J Mate Chem 16:2846–2857
18. Geddes CD, Lakowicz JR (2002) J Fluoresc 12:121–129
19. Li C, Zhu Y, Zhang X, Yang X, Li C (2012) RSC Adv 2:1765–1768
20. Kamat PV, Shanghavi B (1997) J Phys Chem B 101:7675–7679
21. Hummers WS, Offeman RE (1958) J Am Chem Soc 80:1339
22. Cote LJ, Kim F, Huang JX (2009) J Am Chem Soc 131:1043–1049
23. Stankovich S, Dikin DA, Piner RD, Kohlhaas KA, Kleinhammes A, Jia Y, Wu Y, Nguyen ST, Ruoff RS (2007) Carbon 45:1558–1565
24. Clark BJ, Frost T, Russell MA (1993) UV spectroscopy: Techniques, instrumentation, data handling/UV spectrometry group, vol. 4. Chapman & Hall, London
25. ASTM (1985) Zeta potential of colloids in water and waste water. American Society for Testing and Materials, D 4187–4182
26. Eda G, Lin YY, Mattevi C, Yamaguchi H, Chen HA, Chen IS, Chen CW, Chhowalla M (2010) Adv Mater 22:505–509
27. Scholes GD, Rumbles G (2006) Nat Mater 5:683–696
28. Pan DY, Zhang JC, Li Z, Wu MH (2010) Adv Mater 22:734–738
29. Liu HP, Ye T, Mao CD (2007) Angew Chem Int Ed 46:6473–6475
30. Sun X, Liu Z, Welsher K, Robinson J, Goodwin A, Zaric S, Dai H (2008) Nano Res 1:203–212
31. Liz-Marzán LM, Giersig M, Mulvaney P (1996) Langmuir 12:4329–4335
32. Xu YX, Bai H, Lu GW, Li C, Shi GQ (2008) J Am Chem Soc 130:5856–5857